

# Towards Practical Alzheimer’s Disease Diagnosis: A Lightweight and Interpretable Spiking Neural Model

Changwei Wu, Yifei Chen, Yuxin Du, Jinying Zong, Jie Dong,  
Mingxuan Liu, Yong Peng, Jin Fan, Feiwei Qin, Changmiao Wang

**Abstract**—Early diagnosis of Alzheimer’s Disease (AD), especially at the mild cognitive impairment (MCI) stage, is vital yet hindered by subjective assessments and the high cost of multimodal imaging modalities. Although deep learning methods offer automated alternatives, their energy inefficiency and computational demands limit real-world deployment, particularly in resource-constrained settings. As a brain-inspired paradigm, spiking neural networks (SNNs) are inherently well-suited for modeling the sparse, event-driven patterns of neural degeneration in AD, offering a promising foundation for interpretable and low-power medical diagnostics. However, existing SNNs often suffer from weak expressiveness and unstable training, which restrict their effectiveness in complex medical tasks. To address these limitations, we propose FasterSNN, a hybrid neural architecture that integrates biologically inspired LIF neurons with region-adaptive convolution and multi-scale spiking attention. This design enables sparse, efficient processing of 3D MRI while preserving diagnostic accuracy. Experiments on benchmark datasets demonstrate that FasterSNN achieves competitive performance with substantially improved efficiency and stability, supporting its potential for practical AD screening. Our source code is available at <https://github.com/wuchangw/FasterSNN>.

**Index Terms**—Alzheimer’s Disease, Spiking Neural Network, Leaky Integrate-and-Fire Neuron, Bio-Inspired Computing

## I. INTRODUCTION

ALZHEIMER’S Disease (AD) is an irreversible condition that is distinguished by neurodegenerative changes, persistent cognitive decline, and behavioral abnormalities[1]. As the disease advances, patients progressively experience memory deterioration, anxiety, depression, hallucinations, and more psychological manifestations, with severe instances potentially resulting in mortality. The worldwide aging trend has intensified, with the number of AD patients projected to increase from 55 million in 2019 to 139 million by 2050. Numerous patients, especially those in need of long-term

care, not only put plenty of financial and emotional strain on families but also put a great deal of social resource strain on healthcare and senior care services, which presents a serious problem for public health systems worldwide[2]. Usually, AD begins as mild cognitive impairment (MCI)[3] that gradually progresses to severe dementia before reaching the last stage, where people are unable to carry out everyday tasks. Early detection and treatment at the MCI stage, however, may help slow the evolution of the illness and even undo some cognitive impairment. Thus, disease management needs to obtain an accurate early diagnosis of AD at the MCI stage.

Despite the high clinical emphasis on the necessity of early diagnosis, accurate identification of AD, particularly at the MCI stage, remains a significant challenge in actual clinical practice. On one hand, although the widely used Alzheimer’s Disease Assessment Scale-Cognitive Subscale (ADAS-Cog) can effectively evaluate multiple cognitive domains such as memory, language, and executive function, it has limited test items (only 12), lacks sensitivity, and heavily relies on subjective judgment, making it difficult to differentiate the continuous pathological spectrum from MCI to AD accurately [4]. However, although advanced imaging technologies such as structural magnetic resonance imaging (MRI), positron emission tomography / computed tomography (PET-CT), and PET / MR can effectively detect brain atrophy and molecular pathological changes[5], their high costs and dependence on experts significantly limit their widespread clinical application. Non-AD dementias, such as Lewy Body Dementia and Frontotemporal Dementia, have clinical symptoms that highly overlap with those of AD, resulting in a high misdiagnosis rate [6]. This increases the diagnostic burden on physicians and further delays the patient’s access to professional diagnosis and timely intervention.

Despite having a higher specificity in real-world applications, the PET modality’s hefty examination costs put a heavy financial strain on patients and their families. Furthermore, skilled professionals are still needed for diagnostic procedures. As a result, MRI is gradually taking the lead over PET since it is less expensive and offers consistent imaging quality[7–9]. Furthermore, even though cognitive scales are affordable, functional, and simple to use, the consistency and reliability of the scale assessments can be significantly impacted by a patient’s educational background, psychological condition, and regional variations, such as high illiteracy rates in remote places. Thus, creating an assessment technique that blends economic viability and objectivity is imperative. As a modest imaging technique, MRI offers obvious cost and equipment maintenance benefits while maintaining the objectivity of

This work was supported by the Fundamental Research Funds for the Provincial Universities of Zhejiang (No. GK259909299001-006), Anhui Provincial Joint Construction Key Laboratory of Intelligent Education Equipment and Technology (No. IIEET202401), Guangdong Basic and Applied Basic Research Foundation (No. 2025A1515011617, 2022A1515110570) and Innovation Teams of Youth Innovation in Science and Technology of High Education Institutions of Shandong Province (No. 2021KJ088). (Changwei Wu and Yifei Chen contributed equally to this work.) (Corresponding authors: Feiwei Qin, Changmiao Wang.)

C. Wu, Y. Du, J. Zong, J. Dong, Y. Peng, J. Fan and F. Qin are with Hangzhou Dianzi University, Hangzhou 310018, China (e-mail: changweiwu02@gmail.com, duyuxin736@gmail.com, zongjinying83@gmail.com, muhen3260@gmail.com, yongpeng@hdu.edu.cn, fanjinhdu.edu.cn, qinfeiwei@hdu.edu.cn).

Y. Chen, M. Liu are with Tsinghua University, Beijing 100084, China (e-mail: justifc03@gmail.com, arktis@qq.com).

C. Wang is with Shenzhen Research Institute of Big Data, Shenzhen, 518172, China (e-mail: cmwangelbert@gmail.com).

medical imaging. In addition, this study only employs MRI unimodal data to prevent subjective interference and resource waste in multimodal fusion, aiming to create a diagnostic model that is more accurate, cost-effective, and readily deployable.

In recent years, artificial intelligence technologies, including intense learning methods, have shown great potential in AD auxiliary diagnosis[10–12], enabling efficient and objective capture of key imaging features such as hippocampal atrophy and frontal lobe abnormalities[13]. However, existing artificial neural network (ANN) models generally suffer from high power consumption and computational resource requirements, severely limiting their widespread application in primary healthcare and resource-limited regions. In contrast, bio-inspired spiking neural networks (SNNs) simulate the pulse discharge mechanism of biological neurons, triggering pulses only when the membrane potential exceeds a threshold, thus significantly reducing redundant computations[14]. However, existing SNN models have limitations in expressive power and training stability, restricting their performance in complex medical tasks.

To overcome the aforementioned bottlenecks, this study proposes a novel hybrid neural network architecture, FasterSNN, which integrates the low-energy characteristics of SNN and the strong expressive power of ANN. FasterSNN integrates Leaky Integrate-and-Fire (LIF) neurons, the FasterNet [15] model, and a pyramid-structured multi-scale feature fusion attention mechanism, enabling efficient extraction and integration of multi-dimensional feature information from MRI, accurately capturing latent pathological features at different stages of AD, thereby significantly improving diagnostic accuracy, especially in the MCI stage. We systematically validated the proposed model on two authoritative databases, ADNI and AIBL. The experimental results indicate that FasterSNN significantly outperforms existing mainstream CNN and Transformer models in classification accuracy (89.44% on the ADNI dataset and 86.41% on the AIBL dataset), while also demonstrating a significant advantage in energy consumption, requiring only 1.15 J. This result reflects the significant advantages of FasterSNN in terms of resource utilization efficiency and potential for practical deployment. Additionally, single-modality MRI further reduces clinical costs, effectively alleviating the economic burden on patients and their families. This study aims to promote the development of more efficient, cost-effective, easily deployable, and interpretable early diagnostic tools for AD, facilitating the effective translation and application of artificial intelligence technologies in the clinical field of neurodegenerative diseases.

## II. RELATED WORK

### A. Research on Alzheimer's Disease Prediction Based on Traditional Clinical Medicine

Traditionally, the early prediction of AD primarily relies on the ADAS-Cog and fluid biomarker testing. The ADAS-Cog scale, proposed by Rosen et al. in 1984, was introduced to address the shortcomings of diagnostic tools at the time. With just 12 assessment items, it systematically covers various

cognitive dimensions such as memory, language, praxis, and orientation. It is now widely used in the clinical assessment of mild to moderate AD patients. However, this scale has poor identification ability for very mild or severe dementia states and cannot effectively distinguish AD from other types of dementia, often leading to misdiagnosis. In terms of biomarker testing, it primarily focuses on the pathological hypotheses of  $\beta$ -amyloid ( $A\beta$ ) and Tau proteins, using the levels of these proteins in cerebrospinal fluid (CSF) and blood to assist in diagnosis. CSF testing is considered the gold standard due to its high sensitivity and specificity; however, it also comes with high equipment costs and technical requirements, limiting its widespread use in primary healthcare institutions. MRI has been widely used in diagnosis due to its lower cost and excellent spatial resolution. It can effectively detect brain atrophy and structural abnormalities. However, the subjectivity of the results and similar signs caused by normal aging, such as widening of the sulci and ventricles affect diagnostic accuracy. Therefore, objective and automated methods have gradually become the focus of subsequent research.

### B. Research on Alzheimer's Disease Prediction Based on Machine Learning Methods

In recent years, researchers have explored machine learning-based automated diagnostic methods to overcome the subjectivity of traditional diagnoses. Magnin et al. [16] used Support Vector Machine (SVM) to classify MRI data, achieving a high accuracy of 94.5%. However, the automation level was limited due to an insufficient sample size and manual delineation of the Region of Interest (ROI). Bi et al. [17] developed a Random SVM clustering model to reduce computational complexity and improve accuracy, but the experimental scale was small, limiting its generalization capability. The Random Forest method proposed by Lebedev et al. [18] achieved high sensitivity and specificity (88.5%/92.0%) on a larger sample size (410 cases), but the model construction was complex. Ortiz et al. [19] combined unsupervised segmentation with Learning Vector Quantization (LVQ) to improve classification accuracy, but it still required complex preprocessing and had low efficiency. Retico et al. [20] and Vichianin et al. [21] attempted MCI recognition based on SVM and three-class methods, but the accuracy and energy consumption were unsatisfactory. Therefore, although machine learning methods have achieved a certain level of automation, accuracy and efficiency still need improvement.

### C. Research on Alzheimer's Disease Prediction Based on Existing Neural Networks

More efficient and accurate AD diagnosis has been made possible with the development of deep learning technologies and the widespread availability of high-performance computing devices. Qiu et al. [22] were the first to propose using FCN networks to generate disease probability maps and classify them by combining non-imaging data, achieving excellent results on multiple public datasets. Furthermore, Kushol et al. [23] developed the ADDFormer model based

on Vision Transformer (ViT), which further enhanced classification accuracy by combining Fourier features with spatial information. Jang et al. [24] proposed the M3T model, which effectively utilizes spatial information in 3D MRI data by integrating Convolutional Neural Network (CNN) and Transformer, demonstrating excellent classification performance. Jiang et al. [25] further proposed the AAGN model based on transfer learning and anatomical attention mechanisms, which provides better inductive bias and interpretability, significantly improving diagnostic accuracy. Additionally, Retico [20] and Ortiz [19] proposed improved methods for SVM and LVQ, optimizing MCI recognition and achieving high classification accuracy.

Even if the ANN models demonstrated great accuracy in trials, real-world applications still have notable limits. On the one hand, using 2D slices results in a significant loss of spatial information, limiting the model's ability to comprehensively analyze the brain's complex structure in real clinical settings. On the other hand, models using complete 3D data, while improving accuracy, are often accompanied by significant parameters, long training times, and high computational resource demands, severely limiting their application and promotion in resource-limited medical areas. This is especially true in primary healthcare settings, where the deployment of such computationally intensive models faces significant challenges.

#### D. Research on Classification Based on Existing Spiking Neural Networks

As the third generation of neural networks, SNN significantly reduce computational energy consumption through the spiking characteristics of biologically-inspired neurons. Turkson et al. [26] were the first to apply SNN to AD classification tasks, significantly improving classification accuracy through a supervised pretraining method. Additionally, Liu et al. [27] developed the Spiking-PhysFormer model, successfully applying SNN to the remote photoplethysmography (rPPG) field, achieving excellent performance and significant energy efficiency improvements. The Spike-SLR model proposed by Lin et al. [28] demonstrated efficient energy consumption characteristics in sign language recognition tasks while maintaining high classification accuracy. However, current SNN methods still face numerous challenges when applied to AD diagnosis tasks. First, SNNs have limited expressive power, and their feature extraction capability and generalization performance often fail to reach the level of traditional CNN and Transformer models when handling complex medical data such as MRI. Secondly, SNN models have poor training stability and convergence, requiring complex training strategies and techniques, which impact their reliability and usability in practical clinical applications. Furthermore, research on SNN models for medical imaging, especially for 3D MRI data, is still limited, and there is a lack of mature and stable model architectures. Therefore, this study aims to combine the energy efficiency advantages of SNNs with the expressive power of traditional neural networks, proposing a hybrid neural network architecture that balances both accuracy and energy efficiency to overcome the shortcomings of existing methods in practical clinical applications.

### III. METHODOLOGY

As shown in Fig 1. This study suggests an SNN model based on multi-scale feature fusion to classify 3D Alzheimer's MRI data. The LIF neurons, the Spike-weighted Attention (SWA) module, the Faster SNN Block, and the Multi-Scale Feature Fusion (MSF) module are the four fundamental modules that comprise the model. The model initially establishes fundamental computational units by utilizing LIF neurons and a membrane potential update mechanism to accomplish sparse computation that is biologically interpretable. The 3D MRI data input undergoes an initial convolutional layer before proceeding to four feature extraction blocks, each composed of Faster SNN Blocks as the backbone network layers. This module adopts a region-adaptive convolution strategy, where different convolution methods are applied to different regions of the feature map, and the features extracted by different convolutions are concatenated together. The SWA module is integrated with matching trainable parameters in each Faster SNN Block, dynamically weighted through pulse channel and spatial attention. The entire network is constructed with the MSF module, creating a four-level pyramid architecture. Cross-layer connections allow for feature reuse, and learnable parameters are utilized to weight and sum each layer's outputs for feature aggregation. Finally, the fused characteristics are fed into the classifier for accurate classification after undergoing temporal averaging.

#### A. Leaky Integrate-and-Fire Neuron

In classification tasks, conventional ANN models encounter a substantial computing overhead and energy consumption because of the high-resolution three-dimensional voxel structure of 3D MRI data. In contrast, SNN models simulate biological neurons' membrane potential update and spike emission mechanisms, allowing information to be transmitted sparsely, in an event-driven manner, significantly reducing computational costs. This study introduces the LIF neurons proposed by Wu et al. [29]. Each time step in this model involves neurons updating their membrane potential by adding the current input after decaying the membrane potential from the previous time step using a decay coefficient. The neuron triggers a spike and resets the membrane potential when the membrane potential surpasses a predetermined threshold. This methodology helps the model more closely approximate the processing manner of biological neural systems and boosts its ability to represent complicated 3D MRI data and its computing efficiency. Additionally, the sparsity of LIF neurons helps the model focus on critical aspects in the data, lowering the risk of overfitting. It offers reliable support for later modules that deal with feature extraction and classification. The membrane potential update and spike emission mechanism of LIF neurons can be expressed as follows:

$$V_t = \lambda V_{t-1} + \frac{1}{T} \sum_{i=1}^T \mathbf{x}_t^{(i)}, \quad (1)$$

$$S_t = \begin{cases} 1 & \text{if } V_t \geq V_{th} \\ 0 & \text{otherwise.} \end{cases} \quad (2)$$

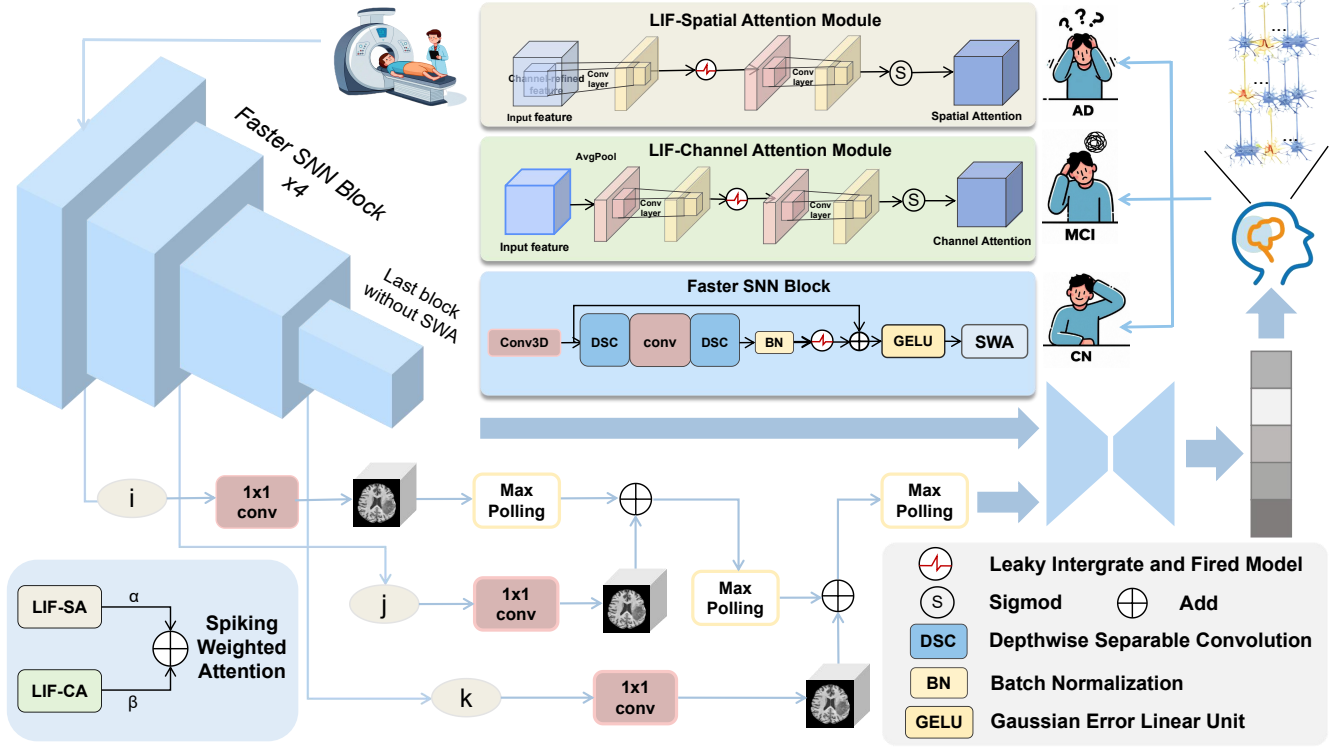


Fig. 1. **The overall architecture of the Faster SNN.** The model consists of multiple Faster SNN blocks. The first three blocks include Depthwise Separable Convolution (DSC), Batch Normalization (BN), Gaussian Error Linear Unit (GELU), and Spiking Weighted Attention (SWA) modules, while the last block excludes the SWA module. The SWA module integrates two types of attention mechanisms: the LIF Spatial Attention and the LIF Channel Attention.

In this context,  $V_t$  represents the membrane potential at time step  $t$ ,  $T$  is the time step (default value is 2),  $\lambda$  controls the decay rate of the membrane potential from the previous time step (initial value is 0.9), and  $V_{th}$  is the spike emission threshold (initial value is 1).  $S_t$  indicates the spike emission state.

### B. Spiking Weighted Attention Module

Pathological characteristics are frequently faint and sparse in 3D Alzheimer's MRI data. Improving classification accuracy requires accurately extracting these important pieces of information and suppressing superfluous voxels. This study uses the LIF neurons to create the SWA module to address this. The module combines the dynamic modeling ability of attention processes with the temporal sparsity of spiking neurons. It enhances the network's perception of important lesion regions by performing fine-grained modeling and weighted changes on the input feature map through parallel pulse channel attention and pulse spatial attention structures.

Specifically, the SWA module aggregates spatial information in the pulse channel attention branch by first performing global average pooling (GAP) on the input feature map, producing a feature representation of size  $(B, C, 1, 1, 1)$ . The number of channels is then reduced to a fourth of their initial size using a  $1 \times 1 \times 1$  convolution to reduce the computational cost. Next, the LIF neuron is implemented for spike discretization to improve information sparsity. Next, another  $1 \times 1 \times 1$  convolution restores the number of channels to the original

dimension, and the channel weight map is output through the Sigmoid activation function. Similarly, the pulse spatial attention branch performs similar operations on the input feature map, ultimately yielding an attention distribution over the spatial dimensions. In order to achieve adaptive adjustment of the dual-path fusion, the SWA module provides two learnable parameters that each govern the percentage of the two types of attention in the final fusion, thereby dynamically balancing the contribution of the two attention mechanisms. The specific formula is as follows:

$$\mathbf{W}_c = \sigma(\text{LIF}(\text{Conv}(\text{GAP}(\mathbf{X})))) , \quad (3)$$

$$\mathbf{W}_s = \sigma(\text{LIF}(\text{Conv}(\text{Conv}(\mathbf{X})))) , \quad (4)$$

$$\mathbf{X}_{\text{out}} = \mathbf{X} \odot (\alpha \mathbf{W}_c + \beta \mathbf{W}_s) , \quad (5)$$

where  $\sigma$  represents the Sigmoid activation function,  $\alpha$  and  $\beta$  represent the weights for channel attention and spatial attention, respectively, with an initial value of 0.5,  $\odot$  indicating element-wise multiplication.

### C. Faster SNN Block

To further improve the model's processing efficiency for 3D high-resolution MRI, this study draws on the region-adaptive concept from FasterNet. It combines it with the LIF neurons to propose the Faster SNN Block. This module uses several convolution techniques to process the input feature map after splitting it into the core and edge areas. While the edge region uses depthwise separable convolution

to save computing strain, the core region uses traditional  $3 \times 3 \times 3$  convolution to extract all feature information. This method successfully strikes a compromise between expressive capabilities and computational overhead while preserving the receptive field. To ensure continuity and consistency in the final concatenated feature map's spatial dimension, the module also provides a spatial masking method that uses the mask matrix  $\mathbf{M}$  to differentiate between the core and edge regions. The module introduces residual connections in the main path to enhance training stability further and mitigate the vanishing gradient problem. It adds sparse features output by the LIF neurons to the residual path, strengthening the feature learning ability. Thanks to the above design, the Faster SNN Block can produce high-quality feature representations for later multi-scale fusion and classification while significantly increasing computing efficiency and accuracy. The specific formula is as follows:

$$\mathbf{F}_{\text{center}} = \text{Conv}_{3 \times 3 \times 3}(\mathbf{X}[:, :, h_s : h_e, w_s : w_e, d_s : d_e]), \quad (6)$$

$$\mathbf{F}_{\text{edge}} = \text{Conv}_{1 \times 1 \times 1}(\text{Conv}_{\text{depthwise}}(\mathbf{X})), \quad (7)$$

$$M_{i,j,k} = \begin{cases} 1 & \text{if } (i, j, k) \in \text{center region} \\ 0 & \text{otherwise,} \end{cases} \quad (8)$$

$$\mathbf{F}_{\text{out}} = \mathbf{M} \odot \mathbf{F}_{\text{center}} + \mathbf{M} \odot \mathbf{F}_{\text{edge}}, \quad (9)$$

$$\mathbf{Y} = \mathbf{X} + \text{LIF}(\text{BN}(\mathbf{F}_{\text{out}})), \quad (10)$$

where  $h_s : h_e, w_s : w_e, d_s : d_e$  represent the starting and ending indices for the height, width, and depth, respectively.  $\text{Conv}_{\text{depthwise}}$  represents depthwise separable convolution.

#### D. Multi-Scale Feature Fusion Module

AD, as a chronic progressive neurodegenerative disease, exhibits distinct multi-scale distribution characteristics in its MRI features. It is challenging for single-scale characteristics to completely display their imaging pattern because it contains both macro-level brain region atrophy and other lesions, as well as micro-level neuronal degeneration traces. The Multi-Scale Feature Fusion Module (MSF) was designed in this work to thoroughly examine multi-scale feature information across layers in response to this characteristic. The MSF module constructs a four-level pyramid structure with channel expansion from 64 to 128, 256, and finally reaching 512 channels. After each layer's output, a  $1 \times 1$  convolution is applied to adjust the output to 64 channels. The outputs of the first three layers are downsampled to the same size via Max Pooling and then added to the fourth layer feature map, achieving spatially aligned fusion. MSF integrates multi-scale features using weighted summation to enhance the cross-layer fusion capability further. Specifically, each layer's feature map is multiplied by a learnable weight after convolution and pooling operations, allowing dynamic adjustment of inter-layer contributions. These weights are automatically optimized during training to fully utilize the discriminative ability of different layers. Finally, the model performs temporal averaging on the fused feature maps from each time step to obtain the final fused feature map, which is then sent to the classifier

to complete the Alzheimer's image classification. The specific formula is as follows:

$$\mathbf{F}_{\text{fusion}} = \sum_{i=1}^N w_i \cdot \text{Pool}(\text{Conv}_{1 \times 1}(\mathbf{X}_{\text{out}})), \quad (11)$$

$$\mathbf{F}_{\text{final}} = \frac{1}{T} \sum_{t=1}^T \mathbf{F}_{\text{fusion}}^{(t)}, \quad (12)$$

where  $w_i$  represents the weight of the feature map at the  $i$ -th layer, with an initial value of 1.0.

## IV. EXPERIMENTS

### A. Dataset

1) *ADNI*: This study combines two Alzheimer's Disease Neuroimaging Initiative (ADNI) data sources to construct a neuroimaging dataset containing three categories: AD, MCI, and CN. Data source one is from the Kaggle public platform and contains 426 images processed to the NIfTI format with a resolution of  $256 \times 256 \times 166$ , including 168 AD patients and 254 CN controls. Data source two was directly obtained from the ADNI platform by our team, and the DICOM data was converted and sequenced using an automated process, resulting in NIfTI images with a spatial resolution of  $256 \times 256 \times 92$ , with 283 MCI cases selected. The entire dataset was stratified and sampled in an 8:2 ratio to build training and testing sets.

2) *AIBL*: This study acquired and processed 682 three-dimensional neuroimaging cases from the Australian Imaging, Biomarker, and Lifestyle (AIBL) platform, including 219 AD cases, 263 MCI cases, and 200 CN controls, with an image spatial resolution of  $160 \times 240 \times 256$ . The entire dataset was stratified and randomly sampled in a 7:3 ratio to form the training and testing sets.

### B. Data Preprocessing

This study resampled all images to a uniform size of  $64 \times 64 \times 64$  and performed Z-score normalization to adapt to the three-dimensional image classification task and improve model training efficiency. Additionally, a temporal sequence with Gaussian noise was generated based on the images, with the output being a PyTorch tensor of shape (Time\_Steps, 64, 64).

### C. Evaluation indicators

This study employs a multidimensional evaluation system to analyze the model from two key perspectives: classification performance and computational efficiency. This approach offers a comprehensive assessment of the overall performance of the model. For measuring classification performance, we utilize standard metrics such as accuracy, precision, recall, and F1-score, along with the Kappa coefficient and average AUC value. These indicators are critical given the issue of dataset imbalance.

$$\text{Accuracy} = \frac{TP + TN}{TP + TN + FP + FN}, \quad (13)$$

$$\text{Precision} = \frac{TP}{TP + FP}, \quad \text{Recall} = \frac{TP}{TP + FN}, \quad (14)$$

$$F1 - score = 2 \times \frac{Precision \times Recall}{Precision + Recall}, \quad (15)$$

$$P_o = \frac{\sum_{i=1}^k n_{ii}}{N}, \quad P_e = \sum_{i=1}^k \left( \frac{n_{i+}}{N} \times \frac{n_{+i}}{N} \right), \quad (16)$$

$$Kappa = \frac{P_o - P_e}{1 - P_e}, \quad AVG \ AUC = \frac{\sum_{i=1}^N n_i \cdot AUC_i}{\sum_{i=1}^N n_i}. \quad (17)$$

Here, TP refers to the number of samples correctly predicted as the positive class, TN refers to the number of samples correctly predicted as the negative class, FP represents the number of samples incorrectly predicted as the positive class, and FN refers to the number of samples incorrectly predicted as the negative class. The accuracy of the prediction is represented by  $P_o$ ,  $P_e$ , indicating the consistency by chance;  $n_{i+}$  refers to the total count of the  $i$ -th class in the accurate labels (row sum), and  $n_{+i}$  refers to the total count of the  $i$ -th class in the predicted labels (column sum).  $AUC_i$  represents the AUC value of the  $i$ -th class.

1) *Energy consumption*: This study introduces a multi-dimensional evaluation system for computational efficiency that includes energy consumption, parameter scale complexity, and training time cost to comprehensively assess the model's resource utilization efficiency.

$$e_{spike} = 77 \times 10^{-15} \text{ J}, \quad e_{mac} = 12.5 \times 10^{-12} \text{ J}, \quad (18)$$

$$MACs = C_{in} \times C_{out} \times k^3 \times W_{out} \times H_{out} \times D_{out}, \quad (19)$$

$$Energy = (MACs \times e_{mac} \times (1 - Sparsity)) + Spikes \times e_{spike}, \quad (20)$$

2) *Parameter amount calculation*: The total number of model parameters is obtained by traversing the trainable parameters (including weights and biases) of all layers in the network and performing an accumulation calculation, with the final result converted to millions (M).

$$Params = \sum_{l=1}^L \left( W_l^{shape} + b_l^{shape} \right), \quad (21)$$

where  $L$  represents the total number of layers in the network,  $W_l^{shape}$  is the product of the dimensions of the weight parameters of the  $l$ -th layer, and  $b_l^{shape}$  is the product of the dimensions of the bias parameters of the  $l$ -th layer.

3) *Time Calculation*: To measure the training time of each model, we add a timestamp at the start of the training process to mark the beginning, and then obtain another timestamp once the training is completed. The difference between the two timestamps represents the training time for a single epoch.

$$Time_{train} = Time_{end} - Time_{start}, \quad (22)$$

where  $Time_{start}$  is the timestamp at the start of the training loop, and  $Time_{end}$  is the timestamp at the completion of the training.

## D. Experimental Details

In this experiment, we uniformly used the PyTorch 2.4.1 deep learning framework and experimented on a hardware platform equipped with a NVIDIA GeForce RTX 4090 GPU and CUDA 11.8. We specifically adopted a mixed precision training strategy to optimize training efficiency. Regarding data processing, the batch size of the training and test sets was 16. During the training phase, we applied a dynamic random shuffle strategy to enhance the generalizability of the model and configured a 4-thread parallel loader to accelerate the speed of data pre-processing. We selected the Adam algorithm as the optimizer for model optimization and set the initial learning rate to 1e-3. Additionally, we configured the weight decay coefficient to 1e-3 for effective model regularization. Furthermore, we adopted the ReduceLROnPlateau dynamic learning rate decay strategy. If the accuracy on the validation set does not improve for three consecutive epochs, the learning rate is halved to avoid local optima. We also applied global gradient clipping to ensure the stability of the training process. For the LIF neurons, we set the initial time step to 2, the spike firing threshold to 1, and the decay coefficient to 0.9 to simulate the dynamic characteristics of biological neurons.

## E. Comparative Experiments

1) *Classification Performance Analysis*: The suggested model performs better overall than the current advanced models, according to the comparative experimental data displayed in Table I and II. Parts a and c of the findings, for instance, demonstrate that the model uses only two time steps to achieve a high classification accuracy of 0.944 and an average AUC of 0.9854 in the ADNI dataset. It also receives a Kappa coefficient score of 0.8394, suggesting strong reliability. Furthermore, the model demonstrates exceptionally great computational resource usage, as indicated in part b of Table 1, with training time and energy consumption of only 15s and 1.15J, respectively.

Compared to the ResNet series models and the FCN model, the proposed model in this paper shows an improvement in classification accuracy by 2.12–5.64 percentage points, and the AVG AUC increases from 0.9414 (ResNet50), 0.9422 (ResNet101), and 0.9396 (FCN) to 0.9854. Although both the proposed and the ResNet series models introduce residual connections to address the vanishing gradient problem in deep networks, ResNet uses many standard convolutions when processing 3D MRI data, leading to significant energy consumption. In contrast, the proposed model reduces energy consumption by introducing the LIF neurons for feature sparsification and the unique convolutional mode of FasterSNNBlock. The training energy consumption is only 1.15J, much lower than 117.74J and 175.39J for the ResNet series and 271.44J for the pure convolution model FCN, demonstrating a highly efficient energy-to-performance ratio.

Transformer series models such as ViT and M3T, which use self-attention mechanisms, inherently incur high computational costs, and this is even more pronounced with 3D data. The energy consumption of the ViT and M3T models reached 131.94J and 2726.73J, respectively, much higher than

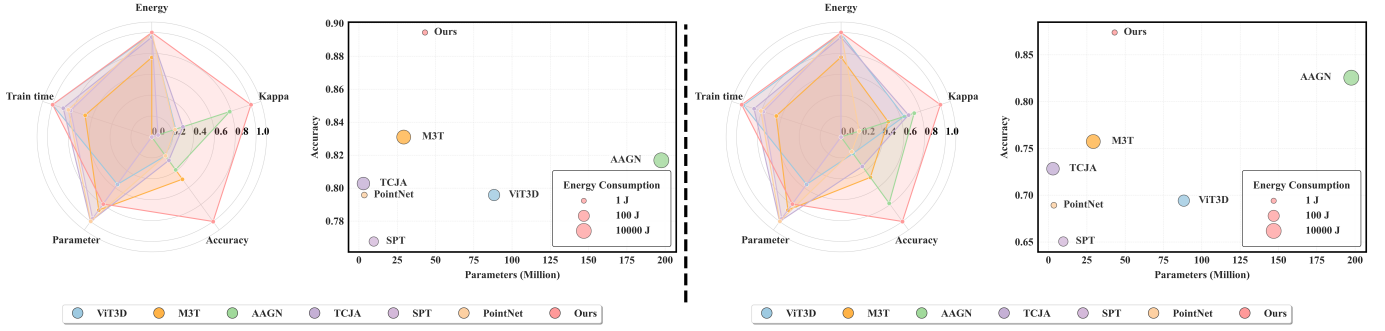


Fig. 2. Performance analysis of various models on the ADNI (left) and AIBL (right) datasets. The radar charts illustrate models’ performance on five metrics: energy, training time, number of parameters, accuracy, and Kappa. Each axis represents one metric, normalized between 0 and 1, with spoke length indicating the relative score. The bubble charts compare models based on energy, parameters, and accuracy. The x-axis shows the number of parameters in millions, the y-axis indicates accuracy, and bubble size reflects energy consumption in joules.

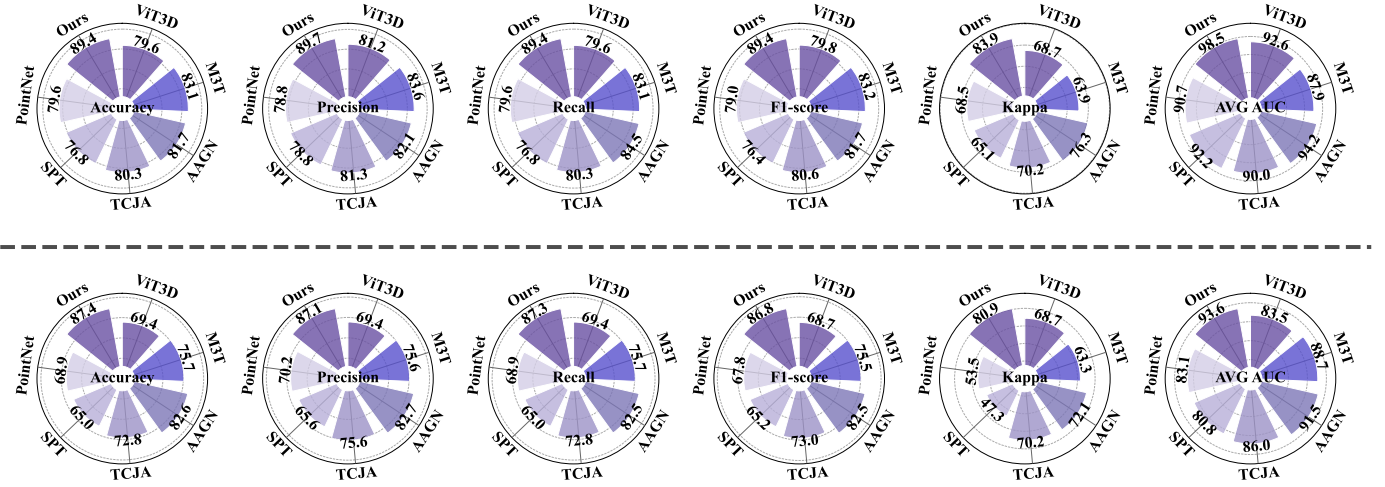


Fig. 3. Classification performance metrics of various models on the ADNI and AIBL datasets. The upper half of the rose plot presents six categorical metrics: accuracy, precision, recall, F1-score, Kappa, and average AUC on the ADNI dataset. The lower half shows the same metrics on the AIBL dataset. All models are clearly labeled and color-coded to facilitate visual comparison.

TABLE I  
COMPARISON OF FASTERSSNN WITH OTHER STATE-OF-THE-ART MODELS ON THE ADNI DATASET.

Model	a						b			c
	Accuracy	Precision	Recall	F1-score	Kappa	AVG AUC	Energy (J)	Train time (s)	Parameter (M)	Time Step
ResNet50[30]	0.8380	0.8392	0.8380	0.8370	0.7516	0.9414	117.74	17	46.16	-
ResNet101[30]	0.8521	0.8569	0.8521	0.8534	0.7738	0.9422	175.39	20	85.21	-
FCN[22]	0.8732	0.8837	0.8732	0.8727	0.8050	0.9396	271.44	19	10.09	-
ViT3D[31]	0.7958	0.8124	0.7958	0.7984	0.6870	0.9261	131.94	15	88.26	-
M3T[24]	0.8310	0.8362	0.8310	0.8321	0.6385	0.8788	2726.73	73	29.23	-
AAGN[25]	0.8169	0.8207	0.8451	0.8169	0.7630	0.9418	11412.47	192	197.51	-
VGGSSNN[32]	0.8169	0.8347	0.8169	0.8205	0.7963	0.9266	602.43	17	10.08	16
ResSNN[33]	0.7183	0.7352	0.7183	0.7197	0.5686	0.8678	1.10	22	5.85	4
TCJA[34]	0.8028	0.8134	0.8028	0.8059	0.7016	0.9003	513.65	34	2.87	16
SPT[35]	0.7676	0.7885	0.7676	0.7638	0.6511	0.9219	19.57	47	9.64	2
PointNet[36]	0.7958	0.7885	0.7958	0.7904	0.6854	0.9068	1.47	43	3.47	16
Ours	0.8944	0.8972	0.8944	0.8943	0.8394	0.9854	1.15	15	43.11	2

the 1.15J of the proposed model. Furthermore, although the proposed model has 43. 11M parameters, which is larger than the 29. 23M parameters of M3T, our model only takes 15 seconds to train, significantly faster than M3T’s 73 seconds. At the same time, the Accuracy and Kappa coefficient of the proposed model reached 0.8944 and 0.8394, respectively, which are much higher than the 0.7958 and 0.6780 for ViT3D,

and the 0.8310 and 0.6385 for M3T. This result indicates that our model performs better in classification and provides more reliable results.

Compared with the AAGN model, the proposed model demonstrates significant energy consumption, training time, and classification performance advantages. Especially in terms of energy consumption, the AAGN model consumes an ex-

TABLE II  
COMPARISON OF FASTER-SNN WITH OTHER STATE-OF-THE-ART MODELS ON THE AIBL DATASET.

Model	a						b			c
	Accuracy	Precision	Recall	F1-score	Kappa	AVG AUC	Energy (J)	Train time (s)	Parameter (M)	Time Step
ResNet50 [30]	0.7864	0.7887	0.7864	0.7862	0.6757	0.9014	104.39	17	46.16	-
ResNet101 [30]	0.7621	0.7891	0.7621	0.7631	0.6423	0.9022	155.50	20	85.21	-
FCN [22]	<b>0.8350</b>	<b>0.8539</b>	<b>0.8350</b>	<b>0.8346</b>	<b>0.7470</b>	<b>0.9174</b>	239.54	19	10.09	-
ViT [31]	0.6942	0.6943	0.6942	0.6866	0.5326	0.8346	116.10	<b>15</b>	88.26	-
M3T [24]	0.7573	0.7563	0.7573	0.7548	0.6327	0.8867	2479.65	68	29.23	-
AAGN [25]	0.8256	0.8266	0.8252	0.8247	0.7209	0.9151	10503.74	173	197.51	-
VGG-SNN [32]	0.7913	0.7916	0.7913	0.7905	0.7245	0.8970	545.80	20	10.08	16
ResSNN [33]	0.5874	0.5893	0.5874	0.5873	0.3546	0.7424	<b>0.97</b>	22	5.85	<b>4</b>
TCJA [34]	0.7282	0.7563	0.7282	0.7297	0.7016	0.8603	465.35	32	<b>2.87</b>	16
SPT [35]	0.6505	0.6557	0.6505	0.6523	0.4732	0.8083	17.78	47	9.64	<b>2</b>
PointNet [36]	0.6893	0.7024	0.6893	0.6776	0.5347	0.8307	1.32	43	<b>3.47</b>	16
Ours	<b>0.8737</b>	<b>0.8714</b>	<b>0.8727</b>	<b>0.8681</b>	<b>0.8094</b>	<b>0.9364</b>	<b>1.01</b>	<b>12</b>	43.11	<b>2</b>

tremely high 11412.47 J, with a training time of 192 seconds. In contrast, the proposed model only uses 1.15J of energy consumption and 15 seconds of training time, yet still achieves classification performance far superior to the AAGN model, particularly in Accuracy and Kappa, where the proposed model significantly outperforms AAGN’s 0.8169 and 0.9418.

In the performance comparison analysis of several SNN models with our model, the proposed model demonstrates outstanding performance on multiple key metrics using only 2 time steps. Although our model has 43.11M parameters, higher than many SNN models, its energy consumption is only 1.15J, similar to ResSNN’s 1.10J and PointNet’s 1.47J, but much lower than VGG-SNN’s 602.43J and TCJA’s 513.65J. This result indicates that our model has higher feature sparsity. In terms of classification accuracy, our model achieved 0.8944, which is significantly higher than many SNN models (ResSNN: 0.7183, PointNet: 0.7958, VGG-SNN: 0.8169, TCJA: 0.8028, and SPT: 0.7676). Additionally, our model achieved 0.9854 in AVG AUC, surpassing all other SNN models.

2) *Confusion Matrix Analysis:* To evaluate the model’s discriminative ability in multi-class classification tasks more intuitively, we plotted confusion matrices on the ADNI and AIBL datasets. By carefully observing the prediction results for each category, we can further reveal the model’s ability to distinguish between different disease stages and its generalization ability. The following will analyze and discuss the model’s performance with the specific classification results.

As shown in Fig 4, the confusion matrix reflects the model’s exceptional performance in the AD classification task. The model excelled in classifying MCI within the ADNI dataset, successfully identifying all 56 samples without misclassification. This highlights the model’s robust ability to detect MCI, a crucial stage for Alzheimer’s intervention and early screening. The model achieved a correct classification rate of 85.7% for the AD category, with 30 samples accurately identified, although 5 were incorrectly classified as CN. The model’s correct classification rate for the CN category was 80.4%, correctly identifying 41 samples while misclassifying 9 as AD and 1 as MCI.

In the AIBL dataset, the model’s recognition rate for the AD category saw a decline. Among the 47 samples identified correctly, 10 were misclassified as MCI, and 7 were misiden-

tified as CN. For the MCI category, the model demonstrated a commendable correct classification rate of 90%, successfully identifying 72 samples, though 4 were misclassified as AD and another 4 as CN. In contrast, the model’s performance in the CN category was remarkable, achieving an accuracy rate of 98.4%, with 59 samples correctly identified and only 3 misclassified as MCI, showcasing the model’s high reliability in recognizing healthy elderly individuals.

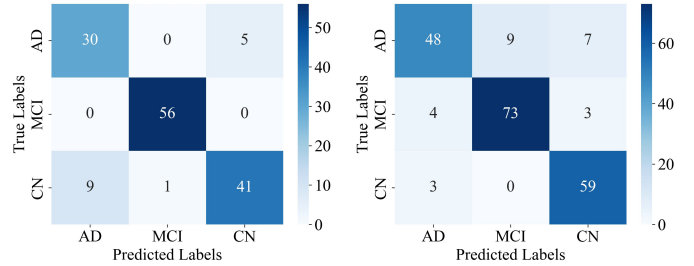


Fig. 4. Confusion matrices of FasterSNN on the ADNI (left) and AIBL (right) datasets, illustrating the model’s performance across different classes.

### F. Ablation Experiments

As shown in Tables III and IV, we conducted an ablation study on the key components of the model in different data sets to assess the specific contribution of each module to the performance of the model. Taking the ablation experiment results on the ADNI dataset as an example, removing the LIF neurons significantly impacted both the model’s performance and energy consumption. From a performance perspective, the model’s classification metrics dropped by 2.82%-4.63%. Among them, the Kappa coefficient experienced the most significant decline, from 0.8394 to 0.7931, indicating a significant reduction in the model’s reliability. This indicates that the membrane potential accumulation mechanism of the LIF neurons can capture more important features. The changes in energy consumption were even more drastic. After losing the feature sparsity provided by LIF neurons, the model’s energy consumption increased from 1.15J to 3.81J, and the training time also increased from 15s to 17s. This is because standard ANN models perform feature extraction through multiple multiply-and-accumulate operations between layers, involving extensive matrix calculations, and thus resulting in high energy consumption. In contrast, SNN models only trigger sparse

spikes from LIF neurons when the membrane potential is high, reducing the computational load. It should be noted that during data loading, the MRI data is processed into a tensor of shape (Time\_Steps, 64, 64, 64). Therefore, after removing the LIF neurons, the model switches to a single time step rather than losing the time step dimension entirely.

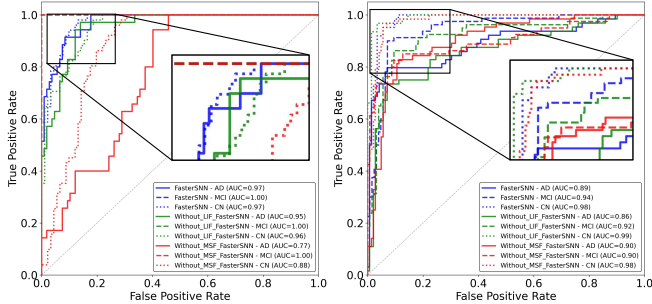


Fig. 5. ROC curves of model ablation experiments on the ADNI (left) and AIBL (right) datasets. The x-axis denotes the false positive rate (FPR), and the y-axis denotes the true positive rate (TPR). Each curve represents a different model configuration, with corresponding AUC values indicated. To highlight performance differences, the upper-left region of each plot is zoomed in.

More notably, the negative impact of removing the MSF module on the model was even greater than that of removing the LIF neurons. From a performance perspective, after removing the MSF module, all metrics showed a severe decline: Accuracy dropped by 14.79% (from 0.8944 to 0.7465), the F1-score dropped by 21.12% (from 0.8943 to 0.6831), and the Kappa coefficient dropped most significantly, from 0.8394 to 0.6082. The drop in the Kappa coefficient indicates that the model no longer has sufficient reliability. Regarding energy consumption, although removing the MSF module reduced the model’s parameter count by 0.06M, it was insufficient to compensate for the performance loss. Additionally, since the LIF neurons promote feature sparsity, reducing computational load and energy consumption from removing the MSF module is minimal. Therefore, the reduction in energy consumption from removing the MSF module cannot be observed when rounding to two decimal places.

This study demonstrates the critical contributions of the LIF neurons and the MSF module through comprehensive ablation experiments. The LIF neurons, employing a sparse pulse-driven computation strategy, enable efficient feature extraction while substantially lowering energy consumption. Meanwhile, the MSF module utilizes a multi-level pyramid structure and a dynamic weighting mechanism to enhance classification performance with minimal increase in model complexity. Notably, these components exhibit strong synergy: the sparse activations from LIF neurons facilitate effective multi-scale feature integration within the MSF module. Their combination leads to significant gains in both accuracy and energy efficiency.

## V. CONCLUSION

In this study, we proposed FasterSNN, a biologically inspired hybrid neural architecture that integrates Leaky Integrate-and-Fire neurons, region-adaptive convolutions, and

a multi-scale spiking attention mechanism. This design effectively addresses key challenges in Alzheimer’s Disease diagnosis, including high energy consumption and poor model interpretability in conventional deep learning approaches. By leveraging the sparse, event-driven nature of spiking neural networks and multi-scale fusion, FasterSNN achieves robust classification performance with significantly reduced computational cost. Experimental results on the ADNI and AIBL datasets demonstrate that FasterSNN outperforms state-of-the-art CNN, Transformer, and SNN models across multiple metrics, achieving superior diagnostic accuracy and efficiency. Ablation studies further validate the essential role of LIF and MSF modules in enhancing both reliability and energy savings. Nevertheless, the current model relies solely on unimodal MRI data and assumes fixed time steps, which may limit its adaptability in more diverse clinical scenarios. In future work, we plan to explore dynamic temporal modeling and multi-modal fusion strategies to further enhance generalizability and clinical applicability.

## REFERENCES

- [1] A. Association *et al.*, “2018 alzheimer’s disease facts and figures,” *Alzheimer’s & Dementia*, vol. 14, no. 3, pp. 367–429, 2018.
- [2] S. Chen, Z. Cao, A. Nandi, N. Counts, L. Jiao, K. Prettnner, M. Kuhn, B. Seligman, D. Tortorice, D. Vigo *et al.*, “The global macroeconomic burden of alzheimer’s disease and other dementias: estimates and projections for 152 countries or territories,” *The Lancet Global Health*, vol. 12, no. 9, pp. e1534–e1543, 2024.
- [3] C. R. Jack Jr, J. S. Andrews, T. G. Beach, T. Buracchio, B. Dunn, A. Graf, O. Hansson, C. Ho, W. Jagust, E. McDade *et al.*, “Revised criteria for diagnosis and staging of alzheimer’s disease: Alzheimer’s association workgroup,” *Alzheimer’s & Dementia*, vol. 20, no. 8, pp. 5143–5169, 2024.
- [4] C. R. Jack Jr, D. A. Bennett, K. Blennow, M. C. Carrillo, B. Dunn, S. B. Haeblerlein, D. M. Holtzman, W. Jagust, F. Jessen, J. Karlawish *et al.*, “Nia-aa research framework: Toward a biological definition of alzheimer’s disease,” *Alzheimer’s & Dementia*, vol. 14, no. 4, pp. 535–562, 2018.
- [5] M. Fan, W. Deng, Y. Zhu, and C. Zhang, “Applications and advances of pet imaging in alzheimer’s disease,” *Int J Radiat Med Nucl Med*, vol. 42, no. 6, pp. 553–558, 2018.
- [6] T. G. Beach, S. E. Monsell, L. E. Phillips, and W. Kukull, “Accuracy of the clinical diagnosis of alzheimer disease at national institute on aging alzheimer disease centers, 2005–2010,” *Journal of Neuropathology and Experimental Neurology*, vol. 71, no. 4, pp. 266–273, 2012.
- [7] C. Zhang, Y. Chen, Z. Fan, Y. Huang, W. Weng, R. Ge, D. Zeng, and C. Wang, “Tc-diffrecon: texture coordination mri reconstruction method based on diffusion model and modified mf-unet method,” in *2024 IEEE International Symposium on Biomedical Imaging (ISBI)*. IEEE, 2024, pp. 1–5.

TABLE III  
ABLATION EXPERIMENTS OF FASTERSSNN ON THE ADNI DATASET.

Model	a						b			c
	Accuracy	Precision	Recall	F1-score	Kappa	AVG AUC	Energy (J)	Train time (s)	Parameter (M)	Time Step
w/o LIF	0.8662	0.8664	0.8662	0.8612	0.7931	0.9529	3.81	17	43.11	1
w/o MSF	0.7465	0.7318	0.7362	0.6831	0.6082	0.8967	1.15	15	43.05	2
Ours	0.8944	0.8972	0.8944	0.8943	0.8394	0.9854	1.15	15	43.11	2

TABLE IV  
ABLATION EXPERIMENTS OF FASTERSSNN ON THE AIBL DATASET.

Model	a						b			c
	Accuracy	Precision	Recall	F1-score	Kappa	AVG AUC	Energy (J)	Train time (s)	Parameter (M)	Time Step
w/o LIF	0.8495	0.8485	0.8495	0.8480	0.7802	0.9395	3.34	17	43.11	1
w/o MSF	0.8398	0.8410	0.8398	0.8381	0.7587	0.9148	1.01	15	43.05	2
Ours	0.8737	0.8714	0.8727	0.8681	0.8094	0.9364	1.01	12	textcolorblue43.11	2

- [8] R. Ge, X. Yu, Y. Chen, G. Zhou, F. Jia, S. Zhu, J. Jia, C. Zhang, Y. Sun, D. Zeng *et al.*, “Tc-kanrecon: High-quality and accelerated mri reconstruction via adaptive kan mechanisms and intelligent feature scaling,” *arXiv preprint arXiv:2408.05705*, 2024.
- [9] Y. Chen, B. Zou, Z. Guo, Y. Huang, Y. Huang, F. Qin, Q. Li, and C. Wang, “Scunet++: Swin-unet and cnn bottleneck hybrid architecture with multi-fusion dense skip connection for pulmonary embolism ct image segmentation,” in *Proceedings of the IEEE/CVF Winter Conference on Applications of Computer Vision*, 2024, pp. 7759–7767.
- [10] T. O. Frizzell, M. Glashutter, C. C. Liu, A. Zeng, D. Pan, S. G. Hajra, R. C. D’Arcy, and X. Song, “Artificial intelligence in brain mri analysis of alzheimer’s disease over the past 12 years: A systematic review,” *Ageing Research Reviews*, vol. 77, p. 101614, 2022.
- [11] Z. Fang, S. Zhu, Y. Chen, B. Zou, F. Jia, L. Qiu, C. Liu, Y. Huang, X. Feng, F. Qin *et al.*, “Gfe-mamba: Mamba-based ad multi-modal progression assessment via generative feature extraction from mci,” *arXiv preprint arXiv:2407.15719*, 2024.
- [12] S. Zhu, Y. Chen, S. Jiang, W. Chen, C. Liu, Y. Wang, X. Chen, Y. Ke, F. Qin, C. Wang *et al.*, “Xlstm-hved: Cross-modal brain tumor segmentation and mri reconstruction method using vision xlstm and heteromodal variational encoder-decoder,” in *2025 IEEE 22nd International Symposium on Biomedical Imaging (ISBI)*. IEEE, 2025, pp. 1–5.
- [13] M. Woodward, D. A. Bennett, T. Rundek, G. Perry, and T. Rudka, “The relationship between hippocampal changes in healthy aging and alzheimer’s disease: a systematic literature review,” *Frontiers in Aging Neuroscience*, vol. 16, p. 1390574, 2024.
- [14] M. Liu, J. Gan, R. Wen, T. Li, Y. Chen, and H. Chen, “Spiking-diffusion: Vector quantized discrete diffusion model with spiking neural networks,” in *2024 5th International Conference on Computer, Big Data and Artificial Intelligence (ICCBDAI)*. IEEE, 2024, pp. 627–631.
- [15] J. Chen, S.-h. Kao, H. He, W. Zhuo, S. Wen, C.-H. Lee, and S.-H. G. Chan, “Run, don’t walk: Chasing higher flops for faster neural networks,” in *Proceedings of the IEEE/CVF Conference on Computer Vision and Pattern Recognition*, 2023, pp. 12 021–12 031.
- [16] B. Magnin, L. Mesrob, S. Kinkingnéhun, M. Pélégri-issac, O. Colliot, M. Sarazin, B. Dubois, S. Lehéricy, and H. Benali, “Support vector machine-based classification of alzheimer’s disease from whole-brain anatomical mri,” *Neuroradiology*, vol. 51, pp. 73–83, 2009.
- [17] X.-a. Bi, Q. Shu, Q. Sun, and Q. Xu, “Random support vector machine cluster analysis of resting-state fmri in alzheimer’s disease,” *PLOS One*, vol. 13, no. 3, p. e0194479, 2018.
- [18] A. Lebedev, E. Westman, G. Van Westen, M. Kramberger, A. Lundervold, D. Aarsland, H. Soinen, I. Kloszewska, P. Mecocci, M. Tsolaki *et al.*, “Random forest ensembles for detection and prediction of alzheimer’s disease with a good between-cohort robustness,” *NeuroImage: Clinical*, vol. 6, pp. 115–125, 2014.
- [19] A. Ortiz, J. M. Górriz, J. Ramírez, F. J. Martínez-Murcia, A. D. N. Initiative *et al.*, “Lvq-svm based cad tool applied to structural mri for the diagnosis of the alzheimer’s disease,” *Pattern Recognition Letters*, vol. 34, no. 14, pp. 1725–1733, 2013.
- [20] A. Retico, P. Bosco, P. Cerello, E. Fiorina, A. Chincarini, and M. E. Fantacci, “Predictive models based on support vector machines: Whole-brain versus regional analysis of structural mri in the alzheimer’s disease,” *Journal of Neuroimaging*, vol. 25, no. 4, pp. 552–563, 2015.
- [21] Y. Vichianin, A. Khummongkol, P. Chiewvit, A. Raksthaput, S. Chaichanettee, N. Aoonkaew, and V. Senanarong, “Accuracy of support-vector machines for diagnosis of alzheimer’s disease, using volume of brain obtained by structural mri at siriraj hospital,” *Frontiers in Neurology*, vol. 12, p. 640696, 2021.
- [22] S. Qiu, P. S. Joshi, M. I. Miller, C. Xue, X. Zhou, C. Karjadi, G. H. Chang, A. S. Joshi, B. Dwyer, S. Zhu *et al.*, “Development and validation of an interpretable deep learning framework for alzheimer’s disease classification,” *Brain*, vol. 143, no. 6, pp. 1920–1933, 2020.
- [23] R. Kushol, A. Masoumzadeh, D. Huo, S. Kalra, and Y.-H. Yang, “Addformer: Alzheimer’s disease detection from structural mri using fusion transformer,” in *2022 IEEE*

*19th International Symposium on Biomedical Imaging (ISBI)*. IEEE, 2022, pp. 1–5.

- [24] J. Jang and D. Hwang, “M3t:three-dimensional medical image classifier using multi-plane and multi-slice transformer,” in *Proceedings of the IEEE/CVF Conference on Computer Vision and Pattern Recognition*, 2022, pp. 20 718–20 729.
- [25] H. Jiang and C. Miao, “Anatomy-aware gating network for explainable alzheimer’s disease diagnosis,” in *International Conference on Medical Image Computing and Computer-Assisted Intervention*. Springer, 2024, pp. 90–100.
- [26] R. E. Turkson, H. Qu, C. B. Mawuli, and M. J. Eghan, “Classification of alzheimer’s disease using deep convolutional spiking neural network,” *Neural Processing Letters*, vol. 53, no. 4, pp. 2649–2663, 2021.
- [27] M. Liu, J. Tang, Y. Chen, H. Li, J. Qi, S. Li, K. Wang, J. Gan, Y. Wang, and H. Chen, “Spiking-physformer: Camera-based remote photoplethysmography with parallel spike-driven transformer,” *Neural Networks*, vol. 185, p. 107128, 2025.
- [28] X. Lin, M. Liu, K. Liu, and H. Chen, “Spike-slr: an energy-efficient parallel spiking transformer for event-based sign language recognition,” 2024.
- [29] Y. Wu, L. Deng, G. Li, J. Zhu, and L. Shi, “Spatio-temporal backpropagation for training high-performance spiking neural networks,” *Frontiers in Neuroscience*, vol. 12, p. 331, 2018.
- [30] K. He, X. Zhang, S. Ren, and J. Sun, “Deep residual learning for image recognition,” in *Proceedings of the IEEE Conference on Computer Vision and Pattern Recognition*, 2016, pp. 770–778.
- [31] K. Kunanbayev, V. Shen, and D.-S. Kim, “Training vit with limited data for alzheimer’s disease classification: An empirical study,” in *International Conference on Medical Image Computing and Computer-Assisted Intervention*. Springer, 2024, pp. 334–343.
- [32] S. Gou, J. Fu, Y. Sha, Z. Cao, Z. Guo, J. K. Eshraghian, R. Li, and L. Jiao, “Dynamic spatio-temporal pruning for efficient spiking neural networks,” *Frontiers in Neuroscience*, vol. 19, p. 1545583, 2025.
- [33] Y. Hu, L. Deng, Y. Wu, M. Yao, and G. Li, “Advancing spiking neural networks toward deep residual learning,” *IEEE Transactions on Neural Networks and Learning Systems*, vol. 36, no. 2, pp. 2353–2367, 2024.
- [34] R.-J. Zhu, M. Zhang, Q. Zhao, H. Deng, Y. Duan, and L.-J. Deng, “Tcja-snn: Temporal-channel joint attention for spiking neural networks,” *IEEE Transactions on Neural Networks and Learning Systems*, 2024.
- [35] P. Wu, B. Chai, H. Li, M. Zheng, Y. Peng, Z. Wang, X. Nie, Y. Zhang, and X. Sun, “Spiking point transformer for point cloud classification,” in *Proceedings of the AAAI Conference on Artificial Intelligence*, vol. 39, no. 20, 2025, pp. 21 563–21 571.
- [36] D. Ren, Z. Ma, Y. Chen, W. Peng, X. Liu, Y. Zhang, and Y. Guo, “Spiking pointnet: Spiking neural networks for point clouds,” *Advances in Neural Information Processing Systems*, vol. 36, pp. 41 797–41 808, 2023.